Optically detected electron-nuclear double resonance of the $S=1$ excited state of the P_{Ga}-Y_P defect in GaP: The neighboring ^{31}P and ^{69}Ga and ^{71}Ga shells

H. J. Sun,* C. F. Rong,† and G. D. Watkins
Department of Physics 16, Lehigh University, Bethlehem, Pennsylvania 18015
(Received 17 May 1994)

Optical detection of electron-nuclear double resonance (ODENDOR) is used to investigate the 1.1-eV photoluminescence of a phosphorus-antisite-related defect in as-grown p-type GaP. We establish that the observed ODENDOR spectra arise from the $M_S=0$ state of a spin $S=1$ excited-state system in which there are no first-order magnetic hyperfine contributions. Nevertheless, including higher-order effects via matrix diagonalization, hyperfine interactions are extracted for the central P and several shells of both P and Ga neighbors, confirming that the defect has a P_{Ga}-Y_P structure, where Y_P denotes an impurity or vacancy at a nearest-neighbor P site. In the case of the Ga neighbors, first-order electric quadrupole interactions are present in the $M_S=0$ manifold and serve to distinguish the three neighbor shells. The excited-state wave function of the defect is highly localized, essentially all of it accounted for within the first-nearest P shell. No ODENDOR signals are observed that can be attributed to Y_P, and its identity remains undetermined.

I. INTRODUCTION

In as-grown p-type GaP, a phosphorus-antisite-related defect, labeled $P_{Ga}Y_P$ (or PP_3Y) has been studied by several groups using optical detection of electron paramagnetic resonance (ODEPR) (Refs. 1–3) and electron-nuclear double resonance (ODENDOR).[4,5] In the ODEPR studies an $S=1$ trigonally distorted spectrum was observed in a luminescence band at ~ 1.1 eV, which revealed resolved hyperfine interactions with a central phosphorus and three equivalent phosphorus neighbors ($^{31}P, I=\frac{1}{2}$). Three different models were proposed: One group suggested that the defect is the isolated P_{Ga} antisite in a C_{3V} Jahn-Teller distorted excited state, the missing P hyperfine interaction (Y_P) resulting from reduced wave function on that site.[2] The other two groups concluded that Y_P is an impurity replacing one of the near-neighbor phosphorus atoms, one[1] suggesting C_P or Si_P, the other[3] Ga_P.

In the first reported ODENDOR study, Shinar *et al.*[4] detected a signal at the normal nuclear resonance frequency for hydrogen and suggested that Y_P might be hydrogen. [They also suggested the alternative interpretation that distant hydrogen was being detected, implying a large concentration of hydrogen in the liquid-encapsulated Czochralski–(LEC-)grown material.] In our subsequent ODENDOR study,[5] a strong signal from the central phosphorus was observed, plus several others that appeared to arise from surrounding phosphorus and gallium neighbors, but no hydrogen or other impurity signals were immediately apparent. As a result, the identity of Y_P and a detailed model for this important defect has remained an unsolved problem.

In our earlier publication[5] we established that the ODENDOR signals were being observed in the $M_S=0$ state with no first-order hyperfine interaction effects, which can substantially reduce the structural information available from ENDOR studies. In that paper, we concentrated therefore primarily on the central phosphorus signal to illustrate the unusual features that occur in that situation where only second- and higher-order effects remain.

In the present paper, we extend the results and analysis to the other observed ENDOR signals. We establish that even though first-order hyperfine interactions are missing, first-order quadrupole interactions remain, which allows the resolution of three inequivalent sets of Ga ($I=\frac{3}{2}$) near neighbors. We find that the remaining ODENDOR signals are all accounted for as arising from P ($I=\frac{1}{2}$) neighbors, second-order magnetic hyperfine effects being large enough to resolve the three equivalent nearest P neighbors plus one additional shell, with the more distant shells contributing to a single line at the normal nuclear-magnetic-resonance frequency for ^{31}P. A careful search reveals no other ODENDOR signals that could arise from an impurity with major abundance nuclear magnetic moment. After presenting these results, their significance as regards the identity of Y_P will be discussed. Several of the models can be discarded. Unfortunately, however, the identity of Y_P remains unknown.

II. EXPERIMENTAL DETAILS

The sample used in this investigation was an as-grown zinc-doped LEC single crystal of GaP, supplied by Kennedy at the Naval Research Laboratory. It was prepared under the same conditions as the sample studied by Shinar *et al.*[4] which was also supplied by Kennedy. The sample dimensions were $0.5\times1.0\times2.0$ mm^3. The dopant concentration was $p=1\times10^{17}$ cm^{-3}.

All experiments were performed in an Oxford Instruments SM-4 optical cryostat with a built-in superconducting magnet and quartz windows allowing operation at pumped liquid-helium temperature (1.7 K). The sam-

0163-1829/94/50(15)/10619(9)/$06.00

ple, mounted on a quartz rod at the end of a long stainless-steel tube, was placed in a 35-GHz TE_{011} microwave cavity designed in the form of concentric rings for optical access and was immersed in the liquid helium (1.7 K) during the experiment.

Photoluminescence (PL) was excited by an Ar^+ laser and detected by a North-Coast EO-817S cooled germanium detector. Optical detection of electron-paramagnetic-resonance spectra were recorded by monitoring changes in the PL intensity synchronous with on-off amplitude modulation of the microwaves as a function of the static magnetic field. For the ODENDOR studies, a two-turn coil was installed in the cavity such that its magnetic-field axis was perpendicular to both the static and microwave magnetic fields. The radio frequency was supplied to the coil from a Fluke 6060B frequency synthesizer amplified by an ENI 3100LA solid-state radio-frequency amplifier. The static magnetic field was tuned to the peak of the ODEPR resonance, and changes in the ODEPR signal intensity were recorded as the radio frequency was swept. The frequency sweep of the synthesizer was computer controlled, and digital signal averaging was performed as necessary.

III. RESULTS

A. Previous ODEPR results (Refs. 1–3)

Figure 1 shows the ODEPR spectrum of the $P_{Ga}Y_P$ center in as-grown p-type GaP with the magnetic field direction parallel to the defect trigonal axis (i.e., $\mathbf{B}\|[111]$). It is observed in a broad emission at ~ 1.1 eV (halfwidth ~ 0.2 eV), and consists of peaks labeled I, II, III, and IV, in the figure (the signal at the center arises from a different defect). The spectrum can be followed only $\sim \pm 30°$ from a particular defect axis before it becomes too weak to be observed, reflecting the breakdown of the radiative "bottleneck" by an off-axis magnetic field, a common feature of excited triplet systems. For this reason, only one of the four equivalently oriented trigonal defects is observed in Fig. 1. The spectrum has been fit over this limited angular range to the first three (S-dependent) terms of the following general $S=1$ spin Hamiltonian

$$\mathcal{H}=g\mu_B\mathbf{B}\cdot\mathbf{S}+D[S_z^2-S(S+1)/3]+\sum_i \mathbf{S}\cdot\mathbf{A}_i\cdot\mathbf{I}_i - \sum_i (\mu_i/I_i)\mathbf{B}\cdot\mathbf{I}_i+\sum_i \mathbf{I}_i\cdot\mathbf{Q}_i\cdot\mathbf{I}_i \ , \quad (1)$$

where for the ith nucleus, $\mathbf{A}_i$ is the hyperfine tensor, μ_i the nuclear moment, and $\mathbf{Q}_i$ the electric quadrupole interaction tensor, required for $I_i>\frac{1}{2}$. Here, $i=0$ for the central P_{Ga} nucleus, $i=1$ for the nearest P neighbors, etc. The analysis is illustrated in Fig. 1, and the values deduced for g, D, and $(A_0)_\|$ are given in Table I. The partially resolved 1:3:3:1 structure on each line reveals additional hyperfine interaction with three equivalent $i=1$ nearest P neighbors, as shown in Fig. 1 with $m_1=\sum_{j=1}^{3} m_j$ giving the nearest-neighbor hyperfine splitting $|\hat{\mathbf{z}}\cdot\mathbf{A}_1|=201$ MHz, where $\hat{\mathbf{z}}$ is the defect $\langle 111\rangle$ axis. This is not given in the table but will be used later in the ODENDOR analysis of $\mathbf{A}_1$. Our previous ODENDOR study[5] supplied the value for $(A_0)_\perp$ given in Table I.

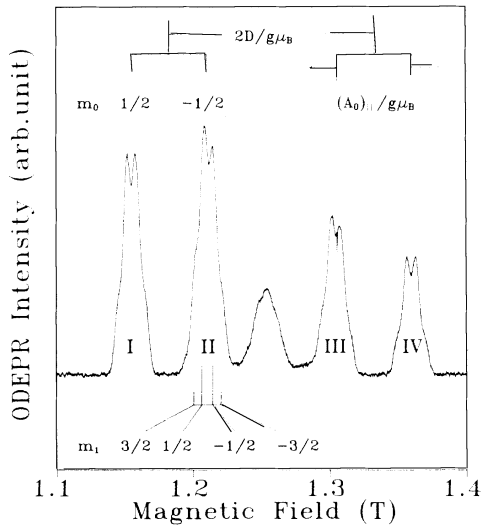

FIG. 1. Optical detection of electron-paramagnetic-resonance spectrum of the $P_{Ga}Y_P$ defect in GaP at $T=1.7$ K, $\nu=35$ GHz, and $\mathbf{B}\|[111]$.

B. Optical detection of electron-nuclear double-resonance results

Figure 2 shows the ODENDOR spectrum with the magnetic field tuned to ODEPR line II of Fig. 1 ($B=1.2$ T), $T=1.7$ K, and $\mathbf{B}\|[111]$. There are several ODENDOR lines observed in the region of 0–25 MHz. In addition, there is a strong line, at ~ 72 MHz, not shown, which we have previously established to arise from the central P_{Ga} nucleus, P_0. No additional ODENDOR signals are observed up to 200 MHz. All of the observed signals are positive, i.e., the ODEPR signal increases at the nuclear magnetic resonances. The ODENDOR resolution is high, with linewidths ~ 0.1 MHz.

In what follows, the analysis of the ODENDOR spectrum for each nucleus will be obtained by matrix diagonalization of Eq. (1) for the appropriate M_S, m_I basis set. However, for illustrative purposes at this stage, it is instructive to consider the first-order solution $(D/g\mu_B B, A_i/g\mu_B B, Q_i/|MA_i-\mu_i B/I_i| \ll 1)$ and for the case of isotropic $\mathbf{A}_i$

$$E\simeq g\mu_B B M_S+D\left[\frac{3\cos^2\theta-1}{2}\right][M_S^2-2/3] +\sum_i [M_S A_i-(\mu_i/I_i)B]m_i +\sum_i (Q_{1i}n_{1i}^2+Q_{2i}n_{2i}^2+Q_{3i}n_{3i}^2)[3m_i^2-I_i(I_i+1)]/2 \ . \quad (2)$$

Here n_{1i}, n_{2i}, n_{3i} are the direction cosines of $\mathbf{B}$ with respect to the 1,2,3 principal axis of the quadrupole ten-

TABLE I. Spin-Hamiltonian parameters for $P_{Ga}Y_P$ ($S=1$, $g=2.007$, and $D=+2151$ MHz). $\tau_{hf}(\tau_Q)$ is the angle between the defect [111] axis and the magnetic hyperfine axis (quadrupole axis) as defined for the (1) axis in Fig. 4.

Atom site (i)	No. of atoms	$A_\parallel$ (MHz)	$A_\perp$ (MHz)	τ_{hf} (degrees)	A (MHz)	Q_{zz} (MHz)	τ_Q (degrees)
Core (0)	^{31}P(1)	+1592	+1304	0			
1 nn (1)	^{31}P(3)	+411	+111	+65±2			
a,c	^{31}P(3)	12	1.5	~−30			
b	^{31}P				<2		
Group I	^{69}Ga(3)				10	2.6	+3
	^{71}Ga(3)				12	1.63	+3
Group II	^{69}Ga(1)				30	0.55	0
	^{71}Ga(1)				34	0.34	0
Group III	^{69}Ga(3)				13	0.33	−38
	^{71}Ga(3)				15	0.22	−38

sor for nucleus i, and θ is the angle between **B** and $\hat{\mathbf{z}}$, the defect ⟨111⟩ axis. This gives for the ENDOR transitions

$$h\nu_i(m_i \rightarrow m_i - 1) \cong |M_S A_i - (\mu_i/I_i)B| + \tfrac{3}{2}(2m_i - 1)(Q_{1i}n_{1i}^2 + Q_{2i}n_{2i}^2 + Q_{3i}n_{3i}^2) . \quad (3)$$

In order to determine the nuclear species responsible for each line in Fig. 2, the ODEPR resonance was shifted to a different value of the magnetic field. The nuclear gyromagnetic ratio (μ_i/I_i) was estimated for each ODENDOR line from its center frequency shift for a change in the magnetic field. This allowed us to identify all transitions shown in Fig. 2, assuming the first-order relation $d\nu_i/dB = \pm\mu_i/I_i h$ from Eq. (3). Signals P_n and P_d are identified with ^{31}P ($d\nu_i/dB = +18.0\pm1.0$ MHz/T). The other signals arise from nearby ^{69}Ga and ^{71}Ga nuclei ($d\nu_i/dB = +10.2\pm0.5$ MHz/T for ^{69}Ga and $+13.0\pm0.5$ MHz/T for ^{71}Ga). As we will demonstrate below, all of these arise from transitions within the $M_S=0$ manifold.

1. P_d lines

There are two different groups of ^{31}P resonances in this region, P_d and P_n. The first, P_d, a single line at ~20.7 MHz for **B**‖[111], is where one would expect the distant phosphorus NMR transition ($\mu B/Ih$). Its magnetic-field dependence is linear and consistent with the ^{31}P gyromagnetic ratio ($\mu/Ih = 17.24$ MHz/T). From Eq. (3), this suggests either that the signal arises from the $M_S=0$ state, or, if it arises from one of the $M_S=\pm1$ states, it must have a vanishingly small value of A_d. The angular dependence reveals that the transition must arise from the $M_S=0$ state, which can be seen as follows.

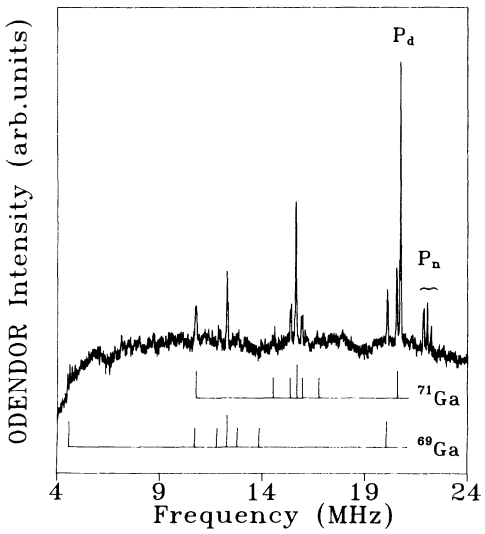

FIG. 2. Optical detection of electron-nuclear double-resonance spectrum when the magnetic field is tuned to ODEPR line II of Fig. 1 ($B=1.2$ T, $T=1.7$ K, **B**‖[111]).

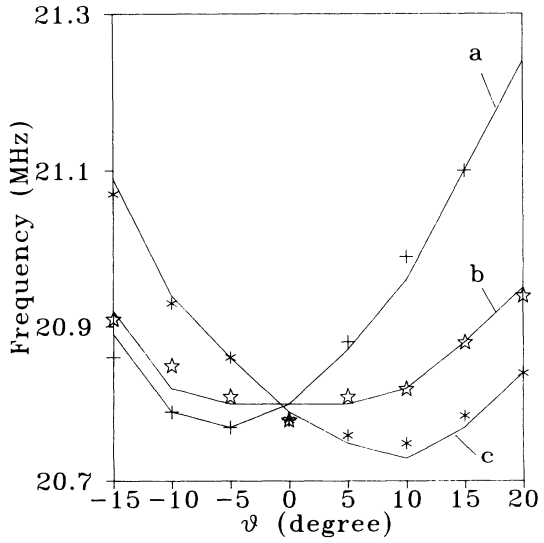

FIG. 3. Dependence of P_d on the angle θ between **B** and the defect [111] axis, as defined in Fig. 4. The solid curves result from matrix diagonalization of Eq. (1) using the parameters of Table I.

As shown in Fig. 3, the single P_d line splits into three lines, labeled *a*, *b*, and *c*, as the magnetic field is rotated away from the [111] defect axis in the $(0\bar{1}1)$ plane. At each angle (θ), the static magnetic field has been readjusted to the new center position of ODEPR resonance II to take account of its angular dependence. These adjustments were small within the $\theta=\pm 15°$ interval over which the ODENDOR signal could be followed, but were necessary to eliminate the unrelated shifts within the line.[5]

$$h\nu_i(m_i\rightarrow m_i-1)\cong\left[\left[\frac{\mu_i}{I_i}B+\frac{A_i^2}{g\mu_B B}\right]^2+\left[\frac{DA_i\sin 2\theta}{g\mu_B B}\right]^2\right]^{1/2}+\tfrac{3}{2}(2m_i-1)(Q_{1i}n_{1i}^2+Q_{2i}n_{2i}^2+Q_{3i}n_{3i}^2)\ . \tag{4}$$

The $DA_i\sin 2\theta$ term produces the additional angular dependence revealing that for the *a* and *c* lines, A_i is not vanishingly small. [As discussed in Ref. 5, this term arises from admixtures of $M_S=\pm 1$ states into the $M_s=0$ state due to off-diagonal *D* terms for $\theta\neq 0$, which provide an effective magnetic field seen by the nucleus which is perpendicular to **B**. There it was shown that comparable fields parallel to **B** can also be induced due to anisotropy in $\mathbf{A}_i$ (not included in our treatment above) which can produce shifts to lower frequencies as well, as evident for the *a* and *c* lines in Fig. 3.]

The curves shown in Fig. 3 are best fits for the ENDOR transitions within the $M_S=0$ state using 12×12 matrix diagonalization of Eq. (1) for the $M_S=0$, ± 1, $m_0=\pm 1$, $m_i=\pm\frac{1}{2}$ product basis sets. In this fit, the (*a*) and (*c*) lines arise from a shell of three equivalent off-axis ^{31}P neighbors with

$$A_\parallel=12\ \text{MHz}\ ,\quad A_\perp=1.5\ \text{MHz}\ ,\quad \tau=-30°$$

and for the *b* line

$$A\leq 2\ \text{MHz}\ .$$

Here τ is the angle between the hyperfine axis and the defect axis, is illustrated in Fig. 4.

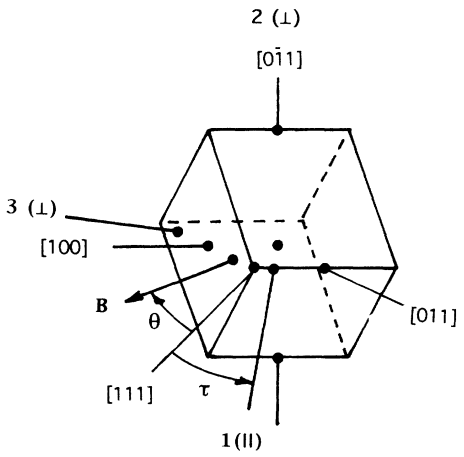

FIG. 4. Coordinate system for the principal axes of the hyperfine and quadrupole tensors. In each case studied here, axial symmetry has either been established or otherwise assumed around the 1 axis, denoted ||, with the corresponding parameters along the 2 and 3 axes taken as equal and denoted ⊥.

The *b* line can be matched well as shown with $\nu=\mu B/Ih$, the curvature resulting from the adjustment in *B*. However, the other two lines of 2(*a*):1(*b*) intensity display a larger angular dependence, coinciding with the central $\nu=\mu B/Ih$ line only for $\mathbf{B}\|[111]$. The origin of this behavior can be seen by augmenting Eq. (2) with additional terms linear in m_i arising from $A_i/g\mu_B B$ and $D/g\mu_B B$ taken to second order, which for the $M_S=0$ state, gives for the ENDOR transitions[5]

2. P_n lines

Figure 5 shows the P_n lines under higher resolution. They consist of three closely spaced groups of lines. An attempt to study their angular dependence failed since they could be followed only in a narrow ($\sim\pm 6°$) angular range between the defect axis and the magnetic-field direction in the $(0\bar{1}1)$ plane. Our analysis shows that they arise from the three nearest phosphorus neighbors. The arguments are as follows. First, they depart slightly from a linear magnetic-field dependence. The 1.3-MHz shift from P_d and the nonlinear field dependence are both satisfactorily accounted for by the $A_i^2/g\mu_B B$ term in Eq. (4) for the $M_S=0$ state with a magnetic hyperfine interaction of ~ 200 MHz, close to that of A_1, as deduced from the ODEPR.

Second, in the case of **B** along the ⟨111⟩ axis of the defect, all three nearest-neighbor phosphorus nuclei are equivalent, having identical hyperfine interactions. In this case, as has been demonstrated in a previous publication,[6] second-order induced pseudo-dipole-dipole interactions[6,7] between the three nuclei cause the resonance to

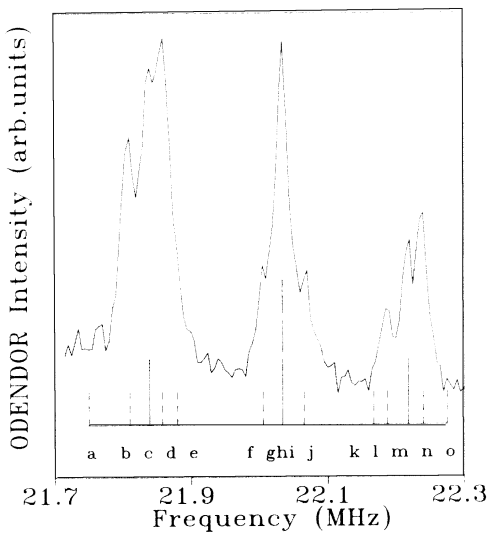

FIG. 5. Optical detection of electron-nuclear double-resonance spectrum for the P_n lines on an expanded scale, $\mathbf{B}\|[111]$. The magnetic field is tuned to ODEPR line II of Fig. 1 ($B=1.2$ T).

split into three lines, with equal spacing, as observed, and with splittings $\sim A_1^2/g\mu_B B$, again consistent with $A_1 \sim 100$ MHz, and the assignment to the $M_S=0$ state.

Assuming axial symmetry for $\mathbf{A}_1$, three parameters are required—$(A_1)_\parallel$, $(A_1)_\perp$, and the angle (τ) between the hyperfine axis and the defect ⟨111⟩ axis, as defined in Fig. 4. Matching to (i) the position of the central ENDOR line, (ii) the splitting between the three, and (iii) the ODEPR-measured hyperfine splitting at this orientation, an accurate determination of these parameters can therefore be made. In our analysis, a 48×48 $[M_S(3)\times m_0(2)\times m_1(8)]$ matrix diagonalization of Eq. (1) was performed. The result, matching the ENDOR transitions for both ODEPR transitions II and I gives $|(A_1)_\parallel|=411\pm1$ MHz, $|(A_1)_\perp|=111\pm1$ MHz (both of the same sign) and $\tau=+65°\pm2°$. [The $\mathbf{P}_1$ hyperfine axis is tilted slightly therefore ($\sim6°$) from the ⟨111⟩ $\mathbf{P}_1$ to $\mathbf{P}_0$ direction, for which τ would be 70.54°].

Additional partially resolved structure is also observed on each of the $\mathbf{P}_n$ lines as shown in Fig. 5. The structure appears as satellites on both sides of each main transition line which are ±0.03 MHz from the main transition line. To understand their origin, consider the nuclear energy-level diagram for the three equivalent nearest P atoms in the $M_S=0$ state, shown in Fig. 6. When $\mathbf{B}$ is along [111] the three P nearest-neighbor nuclei around the $\mathbf{P}_{Ga}$ antisite will be fully equivalent. For this case, there will be two total $I=\frac{1}{2}$ states and one total $I=\frac{3}{2}$ state.

The ENDOR selection rule is $\Delta M_S=0$, $\Delta I=0$, $\Delta m_I=\pm1$. The transitions, labeled *c*, *g*, *h*, *i*, and *m*, and indicated by the solid double arrow lines, are the $\Delta I=0$ allowed ones. The remaining transitions, indicated by the dashed double arrow lines, are forbidden $\Delta I\neq0$ ones. The 48×48 matrix diagonalization analysis shows that the three main lines correspond to the allowed transitions, the satellites arising from the forbidden transitions. The calculated resonance frequencies of the allowed (solid lines) and forbidden (dashed lines) transitions shown in Fig. 5 are identified by the letter designation of Fig. 6. The agreement is satisfactory.

The presence of these forbidden transitions is most likely due either to slight misorientation of the crystal which prevents perfect alignment of $\mathbf{B}\|[111]$, or possibly due to stray fields from neighboring nuclei, either of which would destroy the exact equivalence of the three nearest P nuclei. With the large rf power used in the ODENDOR studies, even weakly allowed NMR transitions can be saturated. Due to the limited resolution and angular dependence data in the ODEPR studies, the complete hyperfine tensor of the three phosphorus nuclei could not be previously obtained. Now, by having carefully analyzed these ODENDOR transitions, an accurate estimate of the hyperfine tensor for the three nearest P nuclei has been possible.

3. *Ga near neighbors*

The ^{69}Ga ($I=\frac{3}{2}$) and ^{71}Ga($I=\frac{3}{2}$) nuclei in the vicinity of the defect can be identified by their electric quadrupole interaction fingerprints. Since, as illustrated in Eq. (4),

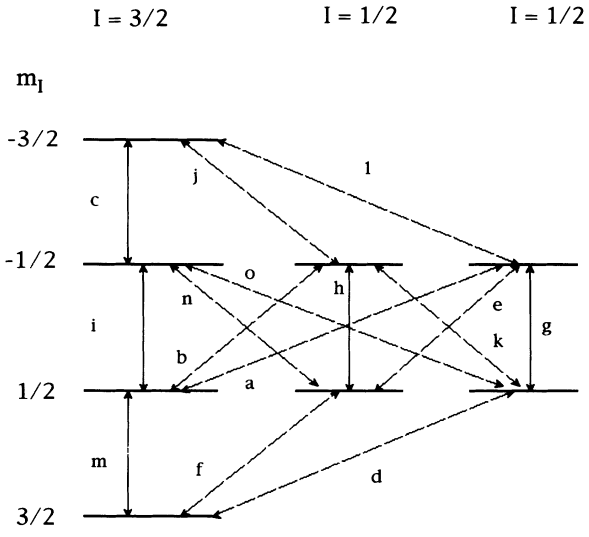

FIG. 6. Nuclear energy-level diagram for the three equivalent nearest P atoms in the $M_S=0$ state, with $\mathbf{B}\|[111]$.

this interaction does not depend on the electronic spin, the first-order contribution from the interaction remains intact in the $M_S=0$ manifold, even when the magnetic hyperfine contributions may be negligible.

The ENDOR transitions, at ~12.3 and ~15.6 MHz, are at $\mu B/Ih$ for ^{69}Ga and ^{71}Ga, respectively, identifying them as the $m=\frac{1}{2}\rightarrow-\frac{1}{2}$ transitions. As indicated in Fig. 2, there are three sets of lines symmetrically placed around each of these central lines and the ratio of their displacements from these lines are given accurately by the quadrupole moment ratios of the two nuclear isotopes. These lines therefore arise from the $m=\frac{3}{2}\leftrightarrow\frac{1}{2}$ and $m=-\frac{1}{2}\leftrightarrow-\frac{3}{2}$ transitions for ^{69}Ga and ^{71}Ga nuclei experiencing three distinctly different quadrupole interactions, labeled I, II, and III, as summarized in Table I.

This close agreement of the applicability of Eq. (3) with no evidence of frequency shifts due to a first-order magnetic hyperfine interaction confirms the identification made above that the transitions arise from the $M_S=0$ state.

Angular dependence studies show that the group-I and group-III lines each split into two lines of 2:1 intensity, as $\mathbf{B}$ is rotated away from the [111] axis in the $(0\bar{1}1)$ plane. This reveals that each arises from a shell of three equivalent off-axis Ga neighbors whose quadrupole axes are tilted symmetrically away from the defect axis by an angle τ in one of the three {110} planes containing the defect ⟨111⟩ axis, as indicated by Fig. 4. The II lines do not split over the $\pm15°$ range by which the ENDOR transitions can be followed, revealing that they arise from a single Ga neighbor situated along the defect ⟨111⟩ axis.

Again, to include second- and higher-order effects, analysis was performed using a 24×24 dimension matrix diagonalization of Eq. (1) $[M_S(3)\times m_0(2)\times m_{Ga}(4)]$. The results, assuming axial symmetry for $\mathbf{Q}_i$ and isotropic A_i, are summarized in Table I.

To check to see if there might be other Ga neighbors not detected because of a larger quadrupole interaction,

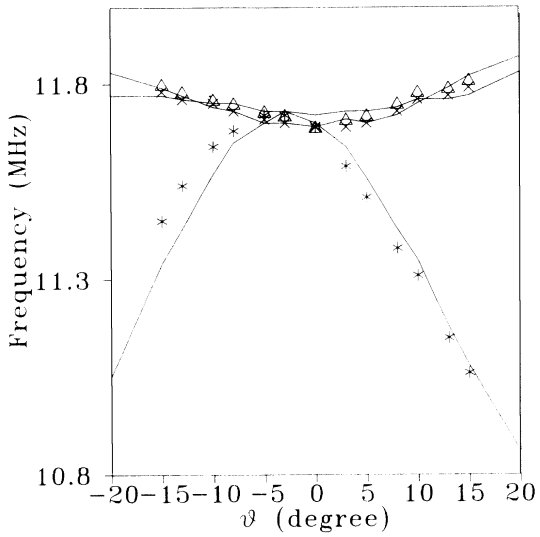

FIG. 7. Angular dependence for the ^{69}Ga ODENDOR $m=+\frac{1}{2}\leftrightarrow-\frac{1}{2}$ transitions with B tuned to ODEPR line I in Fig. 1. The solid curves are calculated from Eq. (1) for the three sets of ^{69}Ga nuclei (Δ, group I; ×, group II; *, group III) using the parameters of Table I.

we explored very carefully the central $m=+\frac{1}{2}\leftrightarrow-\frac{1}{2}$ transition region, where the first-order quadrupole contribution vanishes for all Ga nuclei, to see if all lines were accounted for. Figure 7 shows the angular dependence of the central ^{69}Ga transition lines. The central line splits into three lines when the crystal is rotated away from the defect axis. These three lines are accounted for by the above three groups of gallium nuclei, the triangles for the group I, the crosses for group II, and the stars for the group III. The solid lines are the result of the 24×24 matrix diagonalization using the nuclear Hamiltonian parameters listed in Table I. We conclude therefore that no additional gallium nucleus with a larger electric quadrupole coupling constant exists for the defect. The angular dependence study was also performed on the central ^{71}Ga transition lines. The conclusion is the same. A careful search was also made in the spectral region for hydrogen and for the group-III impurities B, Al, In, and no ODENDOR signals were found.

We conclude therefore that all of the observed ODENDOR transitions arise from the $M_S=0$ state, for which first-order magnetic hyperfine interactions are absent. In spite of this, it has been possible to identify two nearby phosphorus neighbor shells and three of gallium. This provides strong evidence that we have detected all nearby species with nuclear spin $I\neq0$. We conclude therefore that Y_P cannot be an impurity with major abundant nuclear isotope.

IV. DISCUSSION

A. Hyperfine structure

A simple method of representing the electron wave function for a paramagnetic center is using the linear combination of atomic-orbitals (LCAO) approximation. In this method, the one-electron wave function for an unpaired electron is represented by a linear combination of atomic orbitals centered on the atoms near the defect,

$$\Psi=\sum_j \eta_j\psi_j \ , \tag{5}$$

where η_j^2 is the fraction of the electron distribution at the jth atomic site. The atomic orbital is in turn approximately given by a combination of s and p valence orbitals

$$\psi_j=\alpha_j(\phi_{ns})_j+\beta_j(\phi_{np})_j \ , \tag{6}$$

where $(\phi_{ns})_j$ and $(\phi_{np})_j$ denote ns and np valence orbitals at the jth atomic site, respectively. α_j^2 is the fraction of s and β_j^2 the fraction of p orbital, in ψ_j, with $\alpha_j^2+\beta_j^2=1$.

In the approximation that the hyperfine interaction at the jth site is determined primarily by ψ_j, the interaction is axially symmetric along the p-orbital axis and can be written

$$\begin{aligned}(A_{\parallel})_j&=a_j+2b_j \ ,\\ (A_{\perp})_j&=a_j-b_j \ ,\end{aligned} \tag{7}$$

with

$$\begin{aligned}a_j&=\frac{8\pi}{3}g\mu_B(\mu_j/I_j)\alpha_j^2\eta_j^2|(\phi_{ns})_j(0)|^2 \ ,\\ b_j&=\tfrac{2}{5}g\mu_B(\mu_j/I_j)\beta_j^2\eta_j^2\langle r_{np}^{-3}\rangle_j \ .\end{aligned} \tag{8}$$

Our $S=1$ paramagnetic state is made up of two particles—an electron and a hole—for each of which the above LCAO representation can be made. The combined wave function can be aproximated as the antisymmetric product of the one-particle states, which for weakly overlapping two-particle states gives for the $S=1$ hyperfine interaction at nuclear site j, simply the average of the contribution of each particle at that site. Therefore,

$$\begin{aligned}a_j&\cong\frac{(a_j)_e+(a_j)_h}{2} \ ,\\ b_j&\cong\frac{(b_j)_e+(b_j)_h}{2} \ ,\end{aligned} \tag{9}$$

where a_j and b_j apply to the normalized $S=1$ wave function and the analysis can proceed as if it were a single $S=1$ particle state.

As a first method of analysis, we follow the conventional approach and compare a_j and b_j for each site to corresponding estimates for the valence s and p orbitals for the free atom. For ^{31}P we take $a=11\,146$ MHz, and $b=310$ MHz (Ref. 8) and for ^{69}Ga, $a=7430$ MHz, $b=148$ MHz.[9] Using these values, we calculate the molecular wave-function coefficients (η_j^2, α_j^2, and β_j^2) by comparing them to the observed hyperfine parameters, a_j and b_j. The results are given in Table II. By multiplying η^2 by the number of equivalent near neighbor sites N_j, the total fraction of the wave function on the central atom and each near-neighbor shell can be estimated and is given in the last column of the table.

We note that this leads to a total of 146% for the central atom and the first neighbor shell, so something is

TABLE II. Hyperfine parameters (a_j and b_j) and estimates using free-atom values for the corresponding linear combination of atomic orbital–molecular orbital wave-function coefficients for $P_{Ga}Y_P$, compared to those of isolated P_{Ga} (Ref. 11). The estimates shown in bold type were made using a modified free-atom value for the hole contribution, see text, and are believed to be more accurate.

Defect	Atomic site	No. of atoms	a_j (MHz)	b_j (MHz)	$\alpha_j^2\eta_j^2$	$\beta_j^2\eta_j^2$	η_j^2	$N\eta_j^2$
	$^{31}P_0$ (core)	1	1400	96	0.126	0.310	0.436	0.436
					0.126	**0.192**	**0.318**	**0.318**
	$^{31}P_1$ (1 nn)	3	211	100	0.019	0.323	0.342	1.026
					0.019	**0.227**	**0.246**	**0.738**
$P_{Ga}Y_P$ $S=1$	^{71}Ga (I)	3	12		0.002			0.006
	^{71}Ga (II)	1	30		0.004			0.004
	^{71}Ga (III)	3	12		0.002			0.006
	^{31}P (core)	1	2900	0.0	0.260		0.260	0.26
P_{Ga} $S=\frac{1}{2}$	^{31}P (1 nn)	4	224	45	0.020	0.145	0.165	0.66

clearly wrong. For comparison, we also include in Table II a similar analysis for the $S=\frac{1}{2}$ isolated P_{Ga} antisite (PP_4).[10] Here this method of analysis is apparently more realistic, with 92% accounted for on the central atom and the first neighbor P shell. A clue to the problem is to note that the total s character on the central atom ($a_j^2\eta_j^2$) for $P_{Ga}Y_P$ (12.6%) is almost exactly one-half that (26%) for P_{Ga}. This is precisely what we would expect if in the excited state, the electron is on the central antisite P_{Ga}^+ and the hole is bound nearby. This suggests that the electron part of the wave function is being successfully treated by this approach and it is the hole that is not. This is further evidenced by the observation that almost all of the remaining wave function is p-like on the four phosphorus atoms. The top of the valence band is primarily on the phosphorus sublattice and, by symmetry, contains no s character on the atoms, being primarily p. This p character on the P atoms is therefore precisely what is expected for a bound hole.

There is strong evidence that the atomic value estimates for b_j (i.e., $\langle r_{np}^{-3}\rangle$) are underestimated for holelike states in covalent semiconductors. The spin-orbit splitting of the top of the valence band (also a measure of $\langle r_{np}^{-3}\rangle$) is uniformly greater for all semiconductors than the free-atom values. For example, for silicon, the value for the crystal (0.0441 eV) (Ref. 11) is 62% greater than for the free atom (0.0271 eV).[12] For germanium it is 87% greater. The origin of this enhancement has been discussed in more detail in Ref. 8, where it was attributed to a contraction of the wave function around the atomic core for the bonding orbitals associated with the valence band. This suggests therefore that a more realistic estimate of b for a hole on a P atom in the solid would be ~ 310 MHz $\times 1.62 = 500$ MHz, where we take the Si enhancement factor, being adjacent to P in the periodic table. (The spin-orbit splitting for GaP (0.08 eV) (Ref. 11) is a factor of 2 greater than the free-atom value for P (0.040 eV) (Ref. 12) but without a detailed knowledge of the hole wave function, the contribution from the smaller percentage on Ga [with the larger free atom value, 0.102 eV (Ref. 12)] cannot be easily estimated. A direct measure of the enhancement in GaP is therefore not straightforward.)

Shown also in Table II, in bold type, are the results of the analysis with the modified atomic value for phosphorus $b=500$ MHz for the hole part of the wave function. (We have arbitrarily assumed that $\frac{45}{2}$ MHz on the three P neighbors comes from the electron, as indicated for the isolated P_{Ga} results, and for that part we used the free-atom value $b=310$ MHz.) The total wave function now comes out close to 100% (106%), much more reasonable.

Our conclusion from this analysis is therefore that to a good approximation, the excited state can be thought of as P_{Ga}^+ (the unpaired electron) with a hole highly localized nearby on the central and three neighbor P atoms.

B. Model for Y_P

Many models for this defect have been proposed, which we now examine in light of what we have learned. Since we have not found ODENDOR of any impurity, we can conclude that Y_P must be either an intrinsic defect or an impurity with only low abundance nuclear-spin isotopes. Some of the interesting candidates for Y_P such as a hydrogen atom, one of the previously-proposed candidates[4] for Y_P, or a group-III impurity are, therefore, excluded. (Our failure to detect hydrogen conflicts with the ODENDOR study by Shinar *et al.*[4] However, we note that the signals they reported in the 1.1-eV luminescence were *negative* ones and were presumably therefore associated with a competing process in their samples, and not related to the $P_{Ga}Y_P$ emitting center.) There remain several possible models for the defect.

1. Isolated P_{Ga}

As first proposed by Killoran *et al.*,[2] the luminescence could arise from an excited $S=1$ state of the isolated P_{Ga}^0 donor which undergoes a trigonal Jahn-Teller distortion in its excited state with substantially reduced wave function on the on-axis P neighbor. Our analysis of the P_d line establishes that no hyperfine interaction greater than 2 MHz can exist for an on-axis P-near neighbor. As compared with the hyperfine interaction of the three nearest P nuclei, this is a very small interaction. This model therefore is highly unlikely although we cannot of course rule it out completely. However, in their double-excitation experiments, Meyer *et al.*[3] have concluded for other reasons that $P_{Ga}Y_P$ cannot originate from P_{Ga}.

2. P_{Ga}-V_P

The isolated Ga vacancy, V_{Ga}, has been studied theoretically for GaAs by Baraff and Schluter.[13] They predicted that V_{Ga} should exhibit instability as a neighbor As atom moves into the gallium site producing an arsenic vacancy next to an As_{Ga} antisite, As_{Ga}-V_{As}. In their calculation, the defect is converted from V_{Ga} in n-type material to As_{Ga}-V_{As} in p-type material, displaying a strong negative-U property. Similar calculations have not been performed for GaP. The absence of any hyperfine interaction for Y_P is clearly consistent with a P_{Ga}-V_P model. The excited $S=1$ state of the defect might be $(P_{Ga}{}^{+}\text{-}V_P{}^{0})^{+}$, with the ground state of the recombination $(P_{Ga}{}^{0}\text{-}V_P{}^{+})^{+}$. Alternatively, the excited state could possibly be $(P_{Ga}{}^{+}\text{-}V_P{}^{=})^{-}$ with the ground state $(P_{Ga}{}^{0}\text{-}V_P{}^{-})^{-}$, since acceptor as well as the expected donor states have been recently predicted for the anion vacancy in the similar materials GaAs and InP.[14,15] However, since the $(0/+)$ level of isolated P_{Ga} is estimated to be at $\sim E_c$-0.7 eV,[16] and there is no Coulomb interaction between V_P and P_{Ga} in either ground state, this suggests the excited state to be at $>(1.1-0.7)=0.4$ eV above the conduction band edge (assuming that the nearby presence of charged V_P does not substantially alter the single-donor level position of the P_{In} antisite). This model therefore must be considered highly unlikely. (We note that the P_{Ga}-V_P model has previously been proposed[17] for a similar three P-neighbor P_{Ga} antisite center, which we here label by analogy $P_{Ga}X_P$, seen in electron-irradiated GaP by EPR.[18] The question as to whether $P_{Ga}Y_P$ and $P_{Ga}X_P$ are the same center or has not been established, although a tentative conclusion based upon the apparent requirement of electron irradiation to produce the EPR center was that they were not.[1])

3. Group-IV atom

Another suggestion that has been made is that Y_P could be a group-IV single acceptor impurity such as C_P or Si_P[1]. Our ODENDOR results are clearly consistent with this, since group-IV impurities uniformly have low abundance nuclear magnetic isotopes. However, there are problems also with this model. For example, we have $P_{Ga}{}^{++}C_P{}^{-}$ in the ground state. With optical excitation, an electron-hole pair is produced which can be trapped with the hole on the C_P acceptor and the electron on the P_{Ga} donor, resulting in $(P_{Ga}{}^{+}C_P{}^{0})^{+}$. $P_{Ga}{}^{++}C_P{}^{-}$ can certainly bind an electron, but hole binding to the resulting neutral center is difficult according to the normal view since isolated group-IV acceptors are shallow. It should occur only if the hole is trapped deep with a large effective mass m_h. Lattice relaxation of the hole to go deep gives a Stokes shift to lower energy, but this could be compensated by the $\sim 2e^2/\varepsilon r$ Coulomb term. The energy of the transition is about right, being comparable to that for distant P_{Ga}-shallow acceptor pairs [~ 1.2 eV (Ref. 1)]. The relatively sharp $P_{Ga}Y_P$ luminescence centered at 1.1 eV argues against a large contribution from relaxation, however. At the same time, we cannot rule out the possibility that the large strain field of nearby P_{Ga} serves to make it deep.

4. P_{Ga}-Ga_P

Since the defect is a highly-efficient spin-triplet recombination center, a neutral isoelectronic double-donor and double-acceptor structure would be the most logical model. Ga_P, which is an intrinsic double acceptor, would therefore be a logical choice for Y_P. (The alternatives B_P, Al_P, In_P have already been excluded.) This double antisite structure has been proposed by Meyer *et al.*[3] for $P_{Ga}Y_P$, the ground $S=0$ state being $P_{Ga}{}^{++}\text{-}Ga_P{}^{=}$ and the excited $S=1$ state $P_{Ga}{}^{+}\text{-}Ga_P{}^{-}$. However, this gallium, which is adjacent to the P_{Ga} core of the defect, must be on the $\langle 111\rangle$ defect axis and would be expected to display a large electric quadrupole coupling constant. A guide to what we might expect can be obtained from ENDOR studies of the $S=\frac{1}{2}$ neutral single sulfur donor in GaP.[19] The quadrupole interaction for a ^{69}Ga neighbor adjacent to the S core was determined to be $Q_{zz}\sim 7$ MHz. In our case of the P_{Ga} *double donor* core, we might expect an even larger value. Instead, in our study, only one on-axis Ga neighbor (II) was detected and for it, the ^{69}Ga value for Q_{zz} is only 0.55 MHz.

A careful search of the central $m=\frac{1}{2}\leftrightarrow-\frac{1}{2}$ transition regions has ruled out the possibility of any additional Ga neighbor with larger quadrupole interaction. Therefore, unless the quadrupole interaction for a nearest Ga neighbor is unexpectedly small due to accidental cancellation of charge and strain terms, for example, we are forced to reject this attractive model.

V. SUMMARY

An ODENDOR study has been described for the 1.1-eV luminescence associated with the $P_{Ga}Y_P$ center in GaP. We have established that all of the spectra arise from the $M_S=0$ state of its $S=1$ excited state for which there are no first-order magnetic hyperfine contributions. Nevertheless, including higher-order effects by matrix diagonalization, it has been possible to extract these interactions for the central P and several shells of both P and Ga neighbors. In the case of the Ga neighbors, first-order quadrupole interactions are present in the $M_S=0$

manifold and serve to distinguish clearly three neighbor inequivalent sets. An LCAO analysis of the interactions reveals that the excited-state triplet wave function can be considered P_{Ga}^{+} (the unpaired electron), with a hole highly localized on the central and three first neighbor P atoms.

No impurity ODENDOR signals have been observed, revealing that Y_P is either an intrinsic defect or an impurity with low abundance nuclear-spin isotope. This rules out hydrogen, or a group-III impurity such as B, Al, In, etc. A single on-axis Ga atom is observed in the spectrum but its quadrupole interaction is very small, which we argue is inconsistent with a neighbor adjacent to the P_{Ga} double-donor core. Therefore, although the isoelectronic double-donor–double-acceptor P_{Ga}-III_P model is a logical one to explain the highly-efficient luminescence and its deep binding character for both electron and hole, we have been forced to conclude that Y_P is not a group-III atom.

No on-axis P hyperfine interaction is observed with magnetic hyperfine interaction greater than 2 MHz. This is less than 1% of that for the three P neighbors which we argue makes the model of a Jahn-Teller distorted isolated P_{Ga}^{0} ($Y_P = P$) very unlikely.

The models with a phosphorus vacancy or single-acceptor group-IV atom (C_P, Si_P, etc.) as Y_P survive our ENDOR test. However, we have argued that each of these models also has problems, the vacancy model appearing inconsistent with the 1.1-eV luminescence energy, and the group-IV atom perhaps inconsistent with the deep-bound hole.

The identity of Y_P is therefore still undetermined.

---

*Present address: Department of Chemistry, SUNY at Albany, Albany, NY 12222.

†Present address: 26 Deer Trail Drive, Clarksburg, NJ 08510.

[1]K. P. O'Donnell, K. M. Lee, and G. D. Watkins, Solid State Commun. **44**, 1015 (1982).

[2]N. Killoran, B. C. Cavenett, M. Godlewski, T. A. Kennedy, and N. D. Wilsey, J. Phys. C **15**, L723 (1982).

[3]B. K. Meyer, Th. Hangleiter, J.-M. Spaeth, G. Strauch, T. H. Zell, A. Winnacker, and R. H. Bartram, J. Phys. C **18**, 1503 (1985).

[4]J. Shinar, A. Kana-ah, B. C. Cavenett, T. A. Kennedy, and N. D. Wilsey, State Commun. **59**, 653 (1986).

[5]F. C. Rong, H. J. Sun, and G. D. Watkins, Phys. Rev. B **43**, 9108 (1991).

[6]D. Y. Jeon, H. P. Gislason, J. F. Donegan, and G. D. Watkins, Phys. Rev. B **36**, 1324 (1987).

[7]T. E. Feuchtwang, Phys. Rev. **126**, 1628 (1962).

[8]G. D. Watkins and J. W. Corbett, Phys. Rev. **134**, A1359 (1964).

[9]A. K. Koh and D. J. Miller, At. Data Nucl. Data Tables **33**, 235 (1985).

[10]U. Kaufman, J. Schneider, and A. Rauber, Appl. Phys. Lett. **29**, 312 (1976).

[11]K. W. Boer, *Survey of Semiconductor Physics* (Van Nostrand Reinhold, New York, 1990), Vol. I, p. 219.

[12]C. E. Moore, *Atomic Energy Levels,* Natl. Bur. Stand. (U.S.) Circular No. 467 (U.S. GPO, Washington, D.C., 1949).

[13]G. A. Baraff and M. Schluter, Phys. Rev. Lett. **55**, 2340 (1985).

[14]K. Laasonen, R. M. Nieminen, and M. J. Puska, Phys. Rev. **45**, 4122 (1992).

[15]M. Alatalo, R. M. Nieminen, M. J. Puska, A. P. Seitsonen, and R. Virkkunen, Phys. Rev. B **47**, 6381 (1993).

[16]M. Scheffler, J. Bernholc, N. O. Lipari, and S. T. Pantelides, Phys. Rev. B **29**, 3269 (1984).

[17]R. B. Beall, R. C. Newman, J. E. Whitehouse, and J. Woodhead, J. Phys. C **17**, L963 (1984).

[18]T. A. Kennedy and N. D. Wilsey, in *Defects and Radiation Effects in Semiconductors,* edited by J. H. Albany, IOP Conf. Proc. No. 46 (Institute of Physics and Physical Society, London, 1978), p. 375.

[19]B. Utsch, A. Igelmund, and A. Hausmann, Z. Phys. B **30**, 111 (1978).